

Electronic Supplementary Information:

Chemometrics for kinetic investigations of a homogeneously catalysed Sonogashira reaction in flow

Lisa Schulz,^{ab} Mathias Sawall,^c Norbert Kockmann,^a Thorsten Röder^{b*}

^a Laboratory of Equipment Design, Department of Biochemical and Chemical Engineering, TU Dortmund University, 44227 Dortmund, Germany

^b Institute of Chemical Process Engineering, Mannheim University of Applied Sciences, 68163 Mannheim, Germany, *E-mail*: t.roeder@hs-mannheim.de

^c Institute of Mathematics, University of Rostock, 18057 Rostock, Germany

* corresponding author

Table with physical properties	2
Microreactor setup	5
Raman measurements	5
Raman spectra	6
Microreactor characteristics	7
Residence time distribution	7
Heat transfer	8
Heating up the reaction mixture	8
Hot spot estimation	9
Transient flow experiments	10
Multivariate Curve Resolution	11
Applied constraints	11
Kinetic investigations for order in catalyst	14
Supposed catalytic mechanism of the Sonogashira cross-coupling reaction	16
Proposed mechanism explaining half-order dependence of the catalyst	17
Gas chromatography calibration curves	18
NMR Spectroscopy	20
Abbreviations	22
References	23

Table with physical properties

Table S1 Summary of physical property units used for PCA.¹

Property	Units
Melting Point	°C
Boiling Point	°C
Density ^b	g cm ⁻³
Refractive Index ^c	N/A
Dipole Moment	Debye
Dielectric Constant	N/A
Hildebrand Solubility Parameter	(cal cm ⁻³) ^{0.5}
Hansen Parameters (Polar)	(cal cm ⁻³) ^{0.5}
Hansen Parameters (Dispersion)	(cal cm ⁻³) ^{0.5}
Hansen Parameters (Hydrogen-Bonding)	(cal cm ⁻³) ^{0.5}
Solvatochromic – E _T ^N	N/A
Solvatochromic – π*	N/A
Solvatochromic – α	N/A
Solvatochromic – β	N/A
Gutmann Donor Number	kcal mol ⁻¹
log Pow	N/A
Molar Volume	cm ³ mol ⁻¹
Abraham Parameters – AH	N/A
Abraham Parameters – BH	N/A
Abraham Parameters – R2	N/A
Abraham Parameters – Pi	N/A
Abraham Parameters – L ¹⁶ ^d	N/A
Abraham Parameters – V _x	N/A
Auto-Ignition Temperature	°C
Flash Point	°C
Vapor Pressure ^b	mmHg
Water Solubility	g L ⁻¹
Viscosity ^b	cP
Enthalpy of Vaporization ^h	kJ L ⁻¹ ⁱ
Heat Capacity (constant pressure) ^b	J L ⁻¹ K ⁻¹ ^k

Solvent Selection

Based on the solvent selection tool provided by the ACS GCI Pharmaceutical Roundtable¹ we have selected 12 solvents for initial solvent screening. The results can be found in Table S2. It should be noted that the screenings were not performed under isothermal conditions. Therefore, no kinetic data was derived from the obtained yields.

Table S2 Results of the initial solvent screening.

Number on PCA map	solvent	yield 5 min [%]	yield 15 min [%]	yield 60 min [%]	catalyst	reactants
1	triethyleneglycol	29*	41*	45*	not dissolved	dissolved
2	n-propylpropionate	87	92	85	dissolved	not dissolved
3	dimethylformamide	39	64	84	dissolved	dissolved
4	<i>n</i> -methylmorpholine	16	24	44	dissolved	not dissolved
5	diisopropylethylamine	5	7	68	not dissolved	not dissolved
6	ethanolamine	10**	21**	87**	not dissolved	dissolved
7	isopropylamine	54	82	90	dissolved	dissolved
8	triethylamine	33	45	73	dissolved	not dissolved
9	anisole	62	95	95	dissolved	not dissolved
10	propan-2-ol	11	20	27	not dissolved	not dissolved
11	toluene	65	88	88	not dissolved	not dissolved
12	methanol	73	87	90	not dissolved	dissolved

*side product formation was identified, ** solvent and base do not mix, 2 phases

Based on the results of the initial solvent screening, we have selected 12 more solvents for further solvent screening. The results are shown in Table S3.

Table S3 Further Solvent Screening of Sonogashira model reaction

Letter on PCA map	solvent	yield 5 min [%]	yield 15 min [%]	yield 60 min [%]	catalyst	reactants
A	morpholine	32	100	100	not dissolved	not dissolved
B	<i>n</i> -hexylamine***	1	15	81	dissolved	dissolved
C	<i>tert</i> -butylamine	100	100	100	not dissolved	not dissolved
D	isobutylamine	2	28	76	not dissolved	dissolved
E	γ -valerolactone	15	33	52	dissolved	dissolved
F	piperidine	95	97	90	dissolved	not dissolved
G	<i>n</i> -propylamine	3	18	81	not dissolved	dissolved
H	butanol	61	85	88	not dissolved	not dissolved
I	acetone	32	45	66	dissolved	not dissolved
J	tetrahydrofuran	14	54	68	dissolved	not dissolved
K	methylacetate	39	81	80	not dissolved	not dissolved
L	acetonitrile	74	85	86	not dissolved	dissolved

*** *n*-hexylamine was chosen instead of *n*-pentylamine

Unfortunately, γ -valerolactone, which is an environmental friendly, biomass derived solvent bears the disadvantage of relatively high purchasing cost. Table S4 shows the prices of the 4 possible solvents for the Sonogashira reaction (Sigma-Aldrich, $\geq 99.0\%$, 02.2023). Therefore, we have decided to perform kinetic investigations in dimethylformamide. Unfortunately, dimethylformamide is toxic (dermal, inhalative and reproductive) and is not suitable to be used for production processes. Therefore, it should be noted that we recommend using γ -valerolactone as green solvent and consider the investigation of this solvent for the Sonogashira coupling reaction as further work.

Table S4 Pricelist of possible solvents for Sonogashira model reaction

	Product-Nr.	€/L
isopropylamine	471291	17.40
dimethylformamide	D158550	22.84
γ -valerolactone	8.22275	103.25
<i>n</i> -hexylamine	8.04326	160.40

Microreactor setup

The microreactor setup described in the contribution is shown in Figure S1.

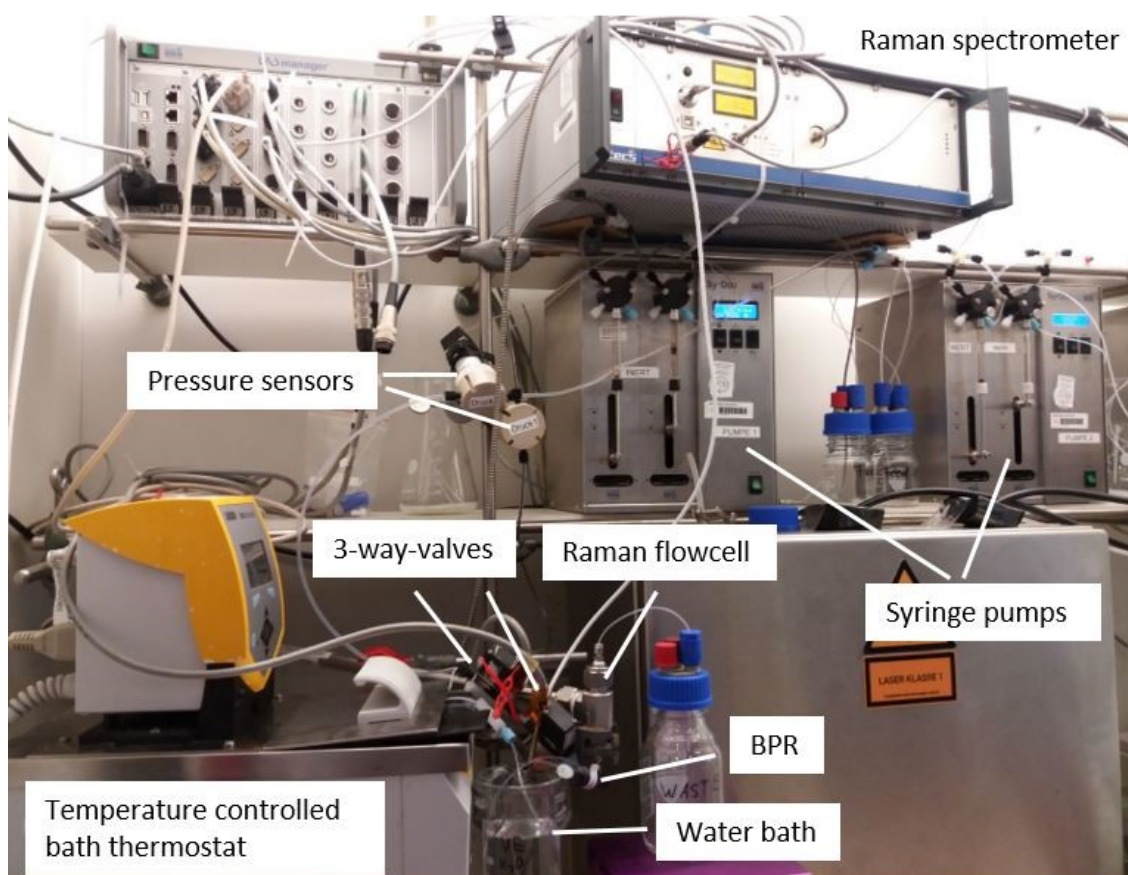


Figure S1 Picture of the microreactor setup in the laboratory environment.

Raman measurements

Raman measurements are performed with a Raman spectrometer (MultiSpec Raman system, Tec5, 785 nm excitation, output power < 500 mW) in a custom build Raman inline flow cell shown in Figure S2. The custom build Raman inline flow cell consists of a reaction Raman probe (InPhotonics, stainless steel sleeve, sapphire window and Kalrez o-ring, 15.9 mm diameter, working distance 1 mm) inserted in a Swagelok T-piece with custom build inlay (inner diameter 1mm). The parameters for the Raman measurements were selected as follows: 12 scans, 1000 ms integration time, 15 seconds cycle time.

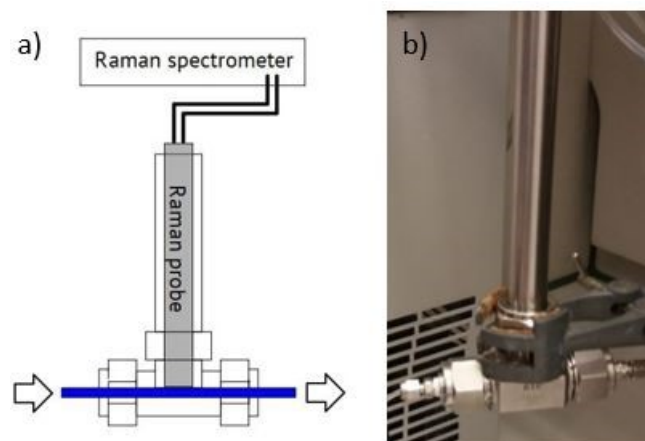


Figure S2 a) Schematic drawing of the custom build Raman flowcell. b) Picture of the custom build Raman flowcell in the laboratory environment.

Raman spectra

The Raman spectra were baseline corrected by designing and minimising a cost function (asymmetric truncated quadratic cost function, 4th polynomial order, threshold 0.01)². The background correction is exemplarily shown in Figure S3.

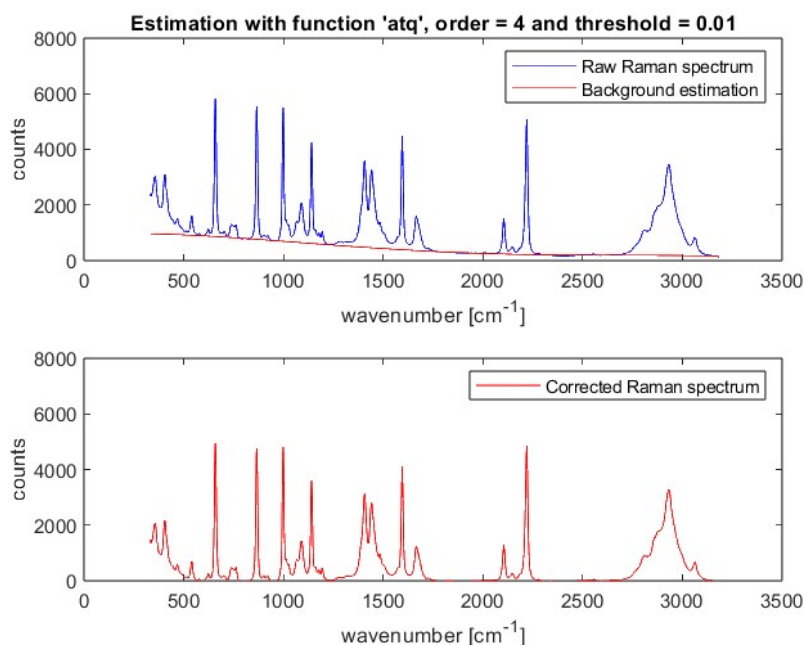


Figure S3 Background correction of Raman spectrum using a asymmetric truncated quadratic (atq) cost function.

Analytical Raman spectra of the Sonogashira reaction over time after baseline correction are exemplarily provided in Figure S4. It can be distinguished between four increasing and decreasing bands. The decreasing band at 2105 cm^{-1} can be assigned to the C-C triple bond of phenylacetylene, while the increasing band at 2222 cm^{-1} belongs to the C-C triple bond of the product. All other

increasing and decreasing bands can be assigned to aromatic ring and aliphatic chain vibrations of phenylacetylene, iodobenzene and product respectively.³

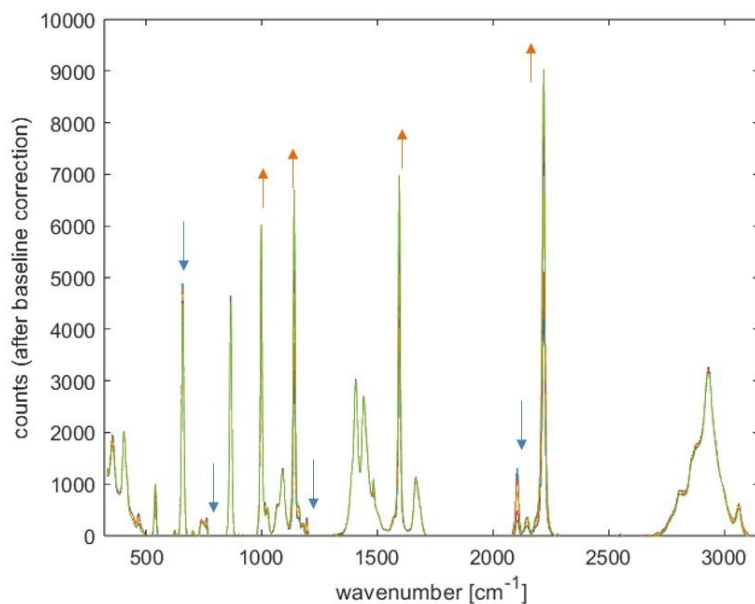


Figure S4 Exemplary Raman spectra of the Sonogashira reaction over time (after baseline correction).

At this point it is important to note, that an investigation with inline FT-IR ATR spectroscopy is not recommended for this reaction, since the C-C triple bond is located on the “blind spot” (2250-1950 cm^{-1}) of the ATR crystal. Furthermore, the C-C triple bond of the product is not IR active.

Microreactor characteristics

Residence time distribution

Table S5 compares the three microreactors applied for kinetic investigations regarding their geometry and the dimensionless Reynolds (Re), Dean (Dn) and Bodenstein (Bo) number. These parameters depend on the flow rate and are exemplarily provided for the lowest and highest value, respectively.

Table S5 Parameter of different microreactors applied for kinetic investigations

Parameter	MR 1		MR 2		MR L	
Channel diameter [mm]	1		0.5		1	
Length [m]	3.18		2.50		10.18	
Inner volume [mL]	2.50		0.49		8	
Flow rate (highest-lowest) [mL min ⁻¹]	1.6	0.16	2	0.16	5	0.5
Residence time (lowest-highest) [min]	1.56	15.6	0.25	3.07	1.60	16.0
Re number (highest-lowest)	34	3	85	7	106	11
Dn number (highest-lowest)	9	1	15	1	27	3
Bo number (lowest-highest) (coiled capillary reactor)	83	311	59	245	106	735

The Bo number is utilized to characterize the degree of backmixing depending on the velocity u , the reactor length L and the axial dispersion coefficient D_{ax} :

$$Bo = \frac{u \cdot L}{D_{ax}} \quad (1)$$

For straight reactor tubes, the axial dispersion coefficient can be calculated through a correlation according to Taylor and Aris.^{4,5} For coiled reactor tubes, D_{ax} can be estimated according to Daskopoulos and Lenhoff.⁶ For high Bo numbers ($Bo > 100$), backmixing can be neglected and plug flow is assumed.⁷ As shown in Table S4 high Bo numbers are achieved, resulting in a narrow residence time distribution. Only in case of the lowest residence time of MR1 and MR2, the Bo number is lower than 100.

Heat transfer

Heating up the reaction mixture

Since the catalyst decomposes during preheating, it was not possible to preheat the educt streams without a tremendous negative impact on the product yield. Therefore, the educt streams were first mixed and afterwards heated to the required temperature. For kinetic modeling it is important to take the time for heating after mixing into account. Table S6 exemplarily shows the required reactor length

and corresponding time for heating up the reaction mixture from 20 °C to 90 °C (MR 1 and MR L) and 100 °C (MR 2), depending on the flow rate. Additionally, the percentage of the overall residence time for heating up is provided, which is just around 2 %. Therefore, the time for heating up can be neglected.

Table S6 Heating time in the different reactors

Parameter	MR 1	MR 2	MR L
Channel diameter [mm]	1	0.5	1
Length [m]	3.18	2.50	10.18
Outer capillary diameter [mm]	1.6	1.6	1.6
Flow rate (highest) [mL min ⁻¹]	1.60	2.00	5
Required length for heating [mm]	67	46	209
Required time for heating [s]	1.98	0.27	1.98
Percent of corresponding residence time required for heating [%]	2.11	1.86	2.06

Hot spot estimation

High heat removal is crucial for achieving nearly isothermal conditions and determining reliable kinetic data. In general, kinetic data is required to estimate the temperature profile in a given reactor, as heat release depends on reaction rate. However, Westermann et al. proposed a shortcut, that can be used as a rough estimation of hot spot generation in the reactor, depending on the inner capillary diameter.⁸ Exemplarily for the investigated (rather exothermic) Sonogashira cross-coupling reaction, hot spot generation was calculated according to this shortcut:

$$\Delta T_{max} = \frac{d^2 \cdot c_0 \cdot (-\Delta H_R)}{14.64 \cdot \lambda \cdot t_{0.5}} \approx 0.11 K \quad (2)$$

with

d	1 mm
c_0	0.5 mol L ⁻¹
$-\Delta H_R$	-130 kJ mol ⁻¹
λ	0.183 W m ⁻¹ K ⁻¹ (pure dimethylformamide)
$t_{0.5}$	231 s

The reaction enthalpy $\Delta_R H$ was calculated from the educt and product formation enthalpies, estimated with the Joback method.⁹

Transient flow experiments

In case of transient flow experiments, the residence time was gradually increased by a constant gradient α , which is calculated as function of the overall experiment time t_{end} :¹⁰

$$\alpha = \frac{V_r}{t_{end}} \left(\frac{1}{Q_{end}} - \frac{1}{Q_0} \right) \quad (3)$$

During the experiment time, Raman measurements (12 scans, 1000 ms integration time, 15 seconds cycle time) are performed. The parameters for the transient flow experiments are provided in the following table.

Table S7 Parameters for transient flow experiments.

	V_r [mL]	τ_0 [min]	\dot{V}_0 [ml min ⁻¹]	τ_{end} [min]	\dot{V}_{end} [ml min ⁻¹]	t_{end} [min]	α	Deviation (lowest τ) [%]	Deviation (highest τ) [%]
MR 1	2.49	1.56	1.6	15.6	0.16	40	0.351	8.75	1.94
MR 2	0.49	0.25	2.0	3.07	0.16	30	0.094	9.58	0.78
MR L	8.00	1.60	5.0	16.0	0.50	40	0.360	5.63	0.56

In the experimental setup, there is a delay volume, V_d , between the reactor exit and the actual Raman measuring point. This delay volume is included in the calculation of the actual residence time that each fluid element spends in the reactor, where t_m is the time when the Raman measurements are performed:¹⁰

$$\tau = (1 - e^{-\alpha}) e^{-\frac{V_d}{V_r}} \left(t_m + \frac{\tau_0}{\alpha} \right) \quad (4)$$

In order to evaluate the time effectiveness of transient flow experiments compared to steady-state experiments, Table S8 compares both approaches regarding experiment time, required volume and number of data points. It becomes evident that transient flow experiments outperform steady-state experiments in all of those three categories. However, it should be noted, that transient flow experiments can only be performed with good results, when a narrow residence times distribution is present.

Table S8 Comparison of steady-state and transient flow conditions.

	Steady-state	Transient flow
Experiment time [min]	75	40
Required volume for reaction [mL]	40	20
Number of data points	4	162

Multivariate Curve Resolution

Applied constraints

MCR can only be performed properly if constraints are applied. Otherwise a nearly infinite number of mathematically possible solutions would arise. This phenomenon is referred to as rotational ambiguity.¹¹ Therefore, constraints relating to the row mode (concentration profiles) were applied.

Table S9 summarizes the applied constraints contrasting soft and hard modeling. Additionally, the effect on the result is described. Regarding hard modeling, there is no need to apply non-negativity, unimodality and local rank information as constraint, since these constraints are already included in the applied kinetic model.

Table S9 Overview of applied constraints.

constraints	soft modeling	hard modeling	effect on result
non-negativity	x	/	no negative concentration values
unimodality	x	/	one single concentration maximum
mass balance closure	x	x	total concentration of the system is fixed to a single value (initial concentration)

kinetic model / x concentration profiles are fit to a kinetic model

Quality parameters

During kinetic investigations as well as the influence of different micromixers and reactor geometry only soft modeling was applied. Therefore, Table S10 shows only the quality parameters of the MCR soft modeling approach. Quality parameters of the of the MCR result contrasting soft and hard modeling are depicted in Table S11. The equations for calculating lack of fit (equation 4) and percent of variance explained (equation 5) are described as followed:

$$R^2 = 100 \sqrt{\frac{\sum_{ij} d_{ij}^2 - \sum_{ij} e_{ij}^2}{\sum_{ij} d_{ij}^2}} \quad (4)$$

$$Lack\ of\ fit\ (\%) = 100 \sqrt{\frac{\sum_{ij} e_{ij}^2}{\sum_{ij} d_{ij}^2}} \quad (5)$$

In those equations, d_{ij} is defined as element of the experimental data matrix D and e_{ij} is the related residue value describing the difference between D and the reproduced data ($C \cdot S^T$).

For the hard modeling approach confidence intervals (95 %) were calculated using the *nlparci* function in MATLAB®. The correlation matrix was calculated from the jacobian matrix.

Table S10 Overview of quality parameters of MCR soft modeling for kinetic investigations.

Experimental data matrix	LoF [%]	R ²
MR L, T Mixer	1.717	99.971
MR 1, Caterpillar mixer	1.284	99.984
MR 1, Static mixing tee	1.165	99.986
MR 1, T Mixer	1.047	99.989
MR 1, X-mixer	0.950	99.991
Preheating	1.224	99.985
Phenylacetylene 0.25 M	0.542	99.997

Phenylacetylene 0.35 M	1.462	99.979
Iodobenzene 0.25 M	0.932	99.991
Iodobenzene 0.35 M	1.204	99.985

Table S11 Overview of quality parameters of MCR soft and hard modeling for estimation of activation energies.

Experimental data matrix	soft modeling		hard modeling	
	Lof [%]	R ²	Lof [%]	R ²
80 °C (CuI = 0.005 M, Pd = 0.0025)	1.235	99.985	1.231	99.992
90 °C (CuI = 0.005 M, Pd = 0.0025)	0.748	99.994	0.761	99.997
100 °C (CuI = 0.005 M, Pd = 0.0025)	1.443	99.979	1.445	99.990
80 °C (CuI = 0.0025 M, Pd = 0.00125)	1.360	99.982	1.349	99.991
90 °C (CuI = 0.0025 M, Pd = 0.00125)	0.957	99.991	0.936	99.996
100 °C (CuI = 0.0025 M, Pd = 0.00125)	1.990	99.960	1.991	99.980

Kinetic investigations for order in catalyst

In order to investigate the order in catalyst, we have varied the catalyst concentration at a constant catalyst ratio ($\text{Pd}(\text{PPh}_3)_4/\text{CuI}$ 1:2). The resulting product concentration profiles are shown in Figure S5. We extrapolated them in order to gain the initial reaction rate, as depicted as black lines. At this point it should be noted, that the retardation of the reaction at low catalyst concentration is not due to side reactions of the educts but rather due to catalyst degradation. A similar effect was reported in literature.¹²

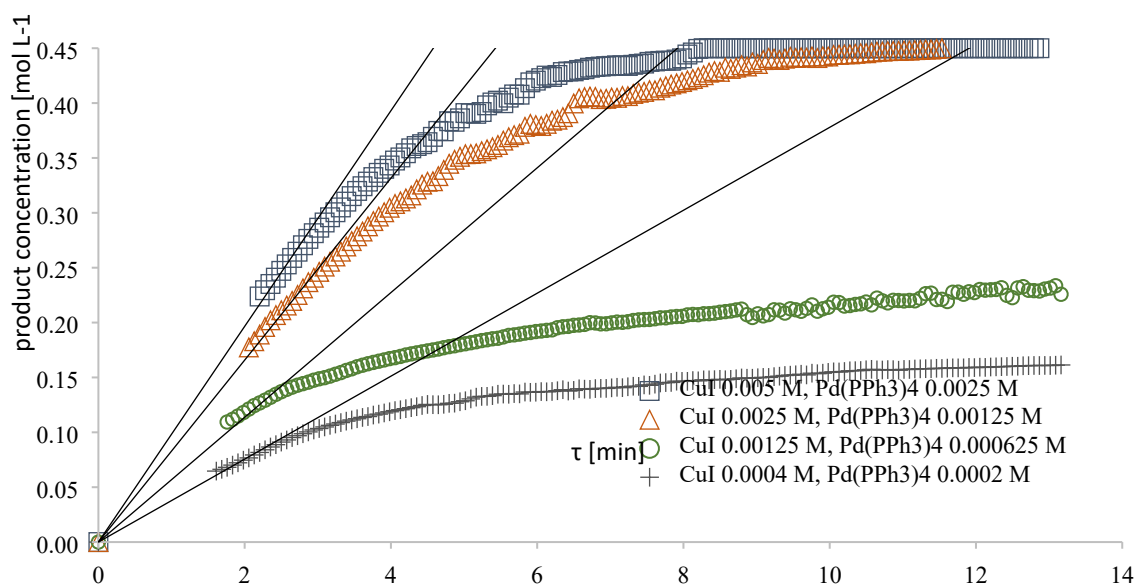


Figure S5 Kinetic profiles of different $\text{Pd}(\text{PPh}_3)_4$ and CuI loadings (ratio 1:2). Reaction conditions: Iodobenzene (0.45 M), Phenylacetylene (0.5 M), $\text{Pd}(\text{PPh}_3)_4$ (0.0025/0.00125/0.000625/0.0002 M), CuI (0.005/0.0025/0.00125/0.0004 M), NEt_3 (1.5 M), 90 °C.

For a more detailed investigation, we focused on the onset of the reaction (residence time 0.25 to 3 minutes) using MR 2. Again, we extrapolated the product concentration profile (see Figure S6) in order to gain the initial reaction rate, as depicted as black lines.

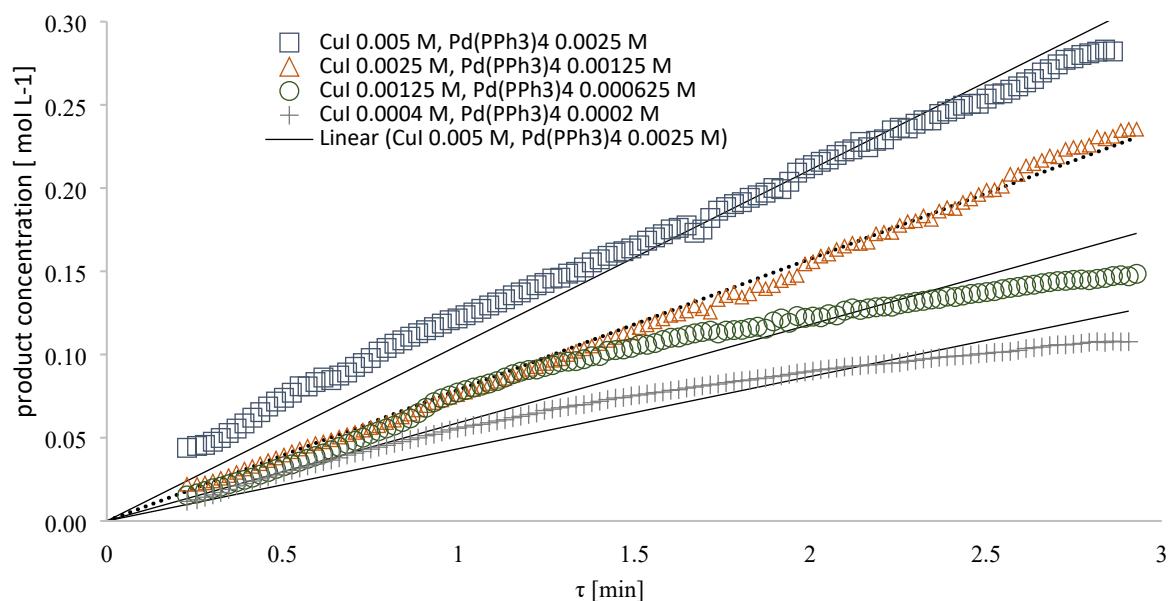


Figure S6 Kinetic profiles of different $\text{Pd}(\text{PPh}_3)_4$ and CuI loadings (ratio 1:2) at the onset of the reaction. Reaction conditions: Iodobenzene (0.45 M), Phenylacetylene (0.5 M), $\text{Pd}(\text{PPh}_3)_4$ (0.0025/0.00125/0.00063/0.0002 M), CuI (0.005/0.0025/0.00125/0.004 M), NEt_3 (1.5 M), 90 °C.

Figure S7 shows the initial rate of reaction (investigated using MR 1 and MR 2) plotted against the square root of the palladium concentration. The linear dependence between the initial rate of reaction and the square root of the palladium concentration results in a fractional order dependence.

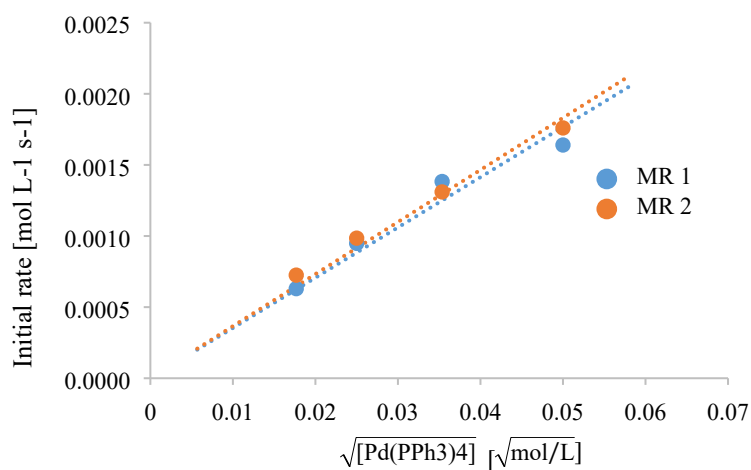


Figure S7 Square root of $\text{Pd}(\text{PPh}_3)_4$ concentration vs. initial concentration. Reaction conditions: Iodobenzene (0.45 M), Phenylacetylene (0.5 M), catalyst ratio 2:1, $\text{Pd}(\text{PPh}_3)_4$ (0.0025/0.00125/0.00063/0.0002 M), CuI (0.005/0.0025/0.00125/0.004 M), NEt_3 (1.5 M), 90 °C.

Supposed catalytic mechanism of the Sonogashira cross-coupling reaction

The exact Sonogashira reaction mechanism is still not very well understood. However, it is generally supposed to take place through two catalytic cycles as shown in Figure S8. The palladium-cycle (cycle A) starts with oxidative addition of an aryl or vinyl halide to the catalytic active species Pd^0L_2 , which can be formed from Pd(0) complexes such as $\text{Pd}(\text{PPh}_3)_4$. The formed adduct is then transformed into a $[\text{Pd}(\text{ii})\text{L}_2\text{R}^1(\text{C}\equiv\text{CR}^2)]$ species after transmetalation with a copper acetylide formed in the copper-cycle (cycle B). This adduct suffers reductive elimination, after *cis/trans*-isomerization, to the final alkyne, regenerating the catalyst $[\text{Pd}^0\text{L}_2]$.¹³

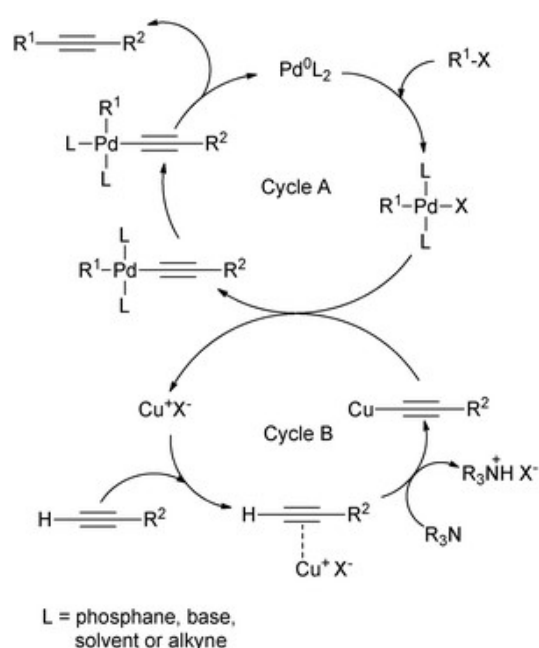


Figure S8 Supposed mechanism for the cross-coupled Sonogashira reaction.¹³

Proposed mechanism explaining half-order dependence of the catalyst

The half-order dependence on the catalyst concentration has already been described in literature for palladium complexes in Heck reactions, which are related to the Sonogashira reactions.^{14,15} The oxidative addition of an aryl halide to the active palladium catalyst (equation 6) species results in the formation of an catalytic active monomer species which is in a fast equilibrium with its off-cycle catalytic inactive dimeric species (equation 8). The supposed mechanism for the Heck coupling reaction including the formation of a catalytic inactive dimeric species $[R^*]$ is shown in Figure S9.

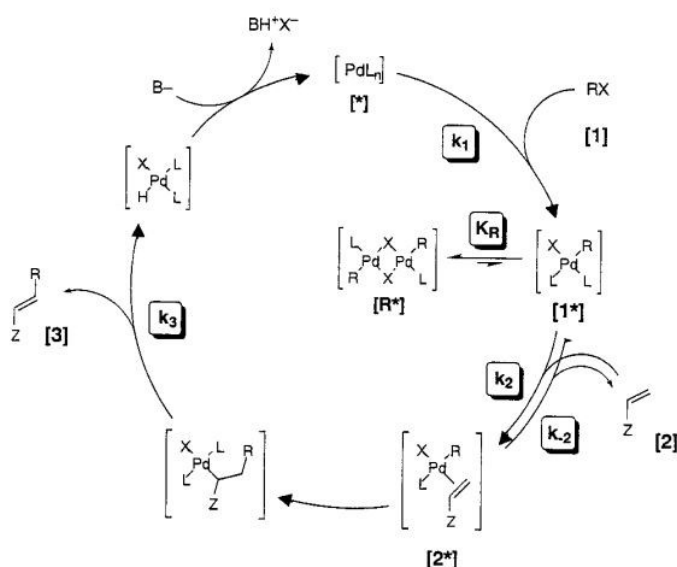
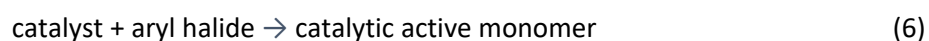


Figure S9 Supposed mechanism for the Heck coupling reaction including the formation of a catalytic inactive dimeric species $[R^*]$.¹⁴

Therefore, we propose the following mechanism for the observed half-order dependence in catalyst:



$$K_R = \frac{[\text{Dimer}]}{[\text{catalytic active monomer}]^2} \quad (8)$$

$$[\text{catalytic active monomer}] = \sqrt{\frac{[\text{Dimer}]}{K_R}} \quad (9)$$

When dimeric species dominate, the concentration of the catalyst active monomer can be expressed by the concentration of dimer species in equilibrium, resulting in a reaction rate that is proportional to the square root of dimer concentration in equilibrium. Assuming that the initial catalyst concentration is equivalent to the dimeric species the kinetic model can be written as follows:

$$\frac{d[P]}{dt} = k_1[Iodobenzene]^0[Phenylacetylene]^1[Catalyst]_0^{0.5} \quad (10)$$

Gas chromatography calibration curves

GC was calibrated using a five-point calibration. The GC oven temperature program was adjusted to an initial temperature of 50 °C for 2 minutes, the temperature was increased at a rate of 40 °C/min over a period of 5 minutes until it reached 200 °C. Then the GC oven was heated at a rate of 10 °C/min over a period of 4 minutes until the final temperature (240 °C) was reached and hold for 2 minute. Afterwards, the oven is cooled down at a rate of 70 °C/min to 100 °C. The injection volume amounts to 1 µL.

The calibration curves are shown in the following figures.

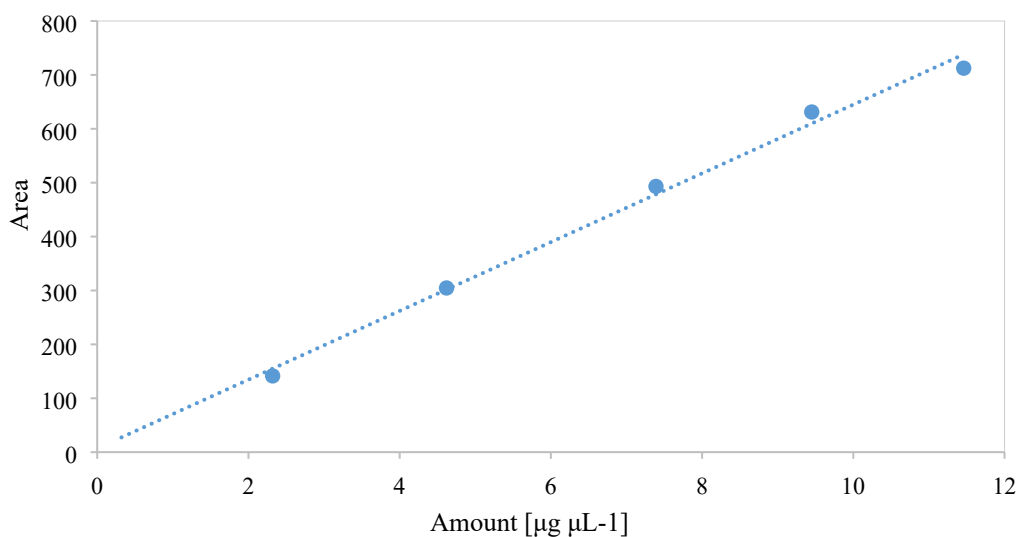


Figure S10 Calibration curve for iodobenzene.

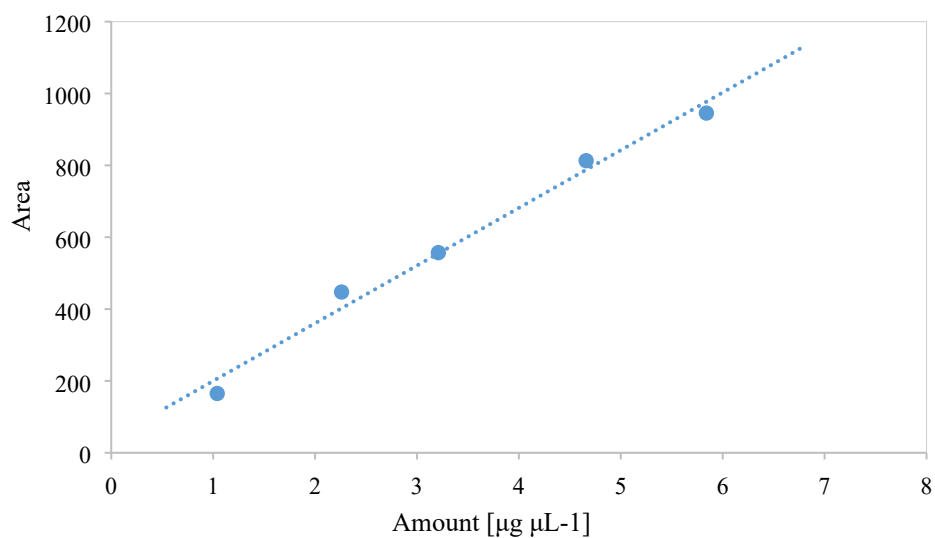


Figure S11 Calibration curve for phenylacetylene.

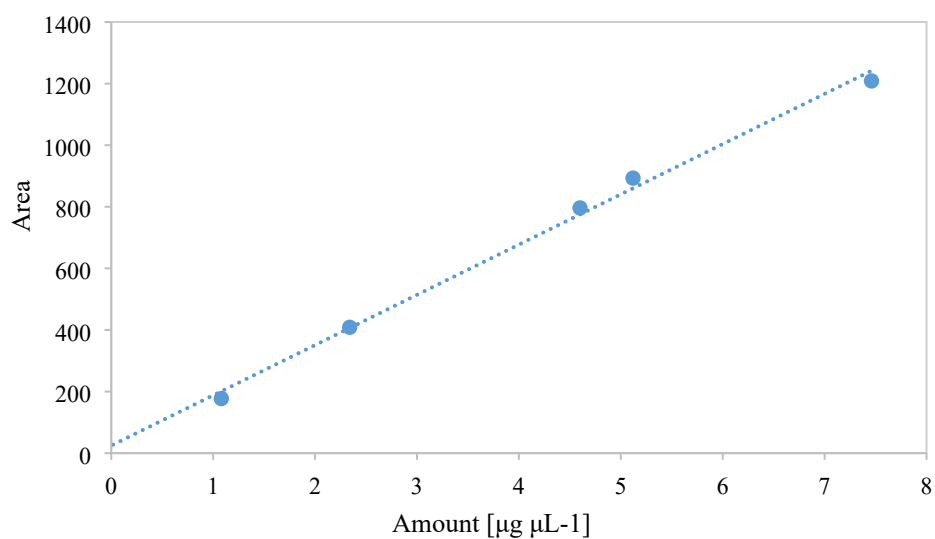


Figure S12 Calibration curve for diphenylacetylene.

Figure S5 shows an exemplary GC run of the reaction mixture at almost full conversion. It should be noted that the amount of the homo-coupled side product 1,4-Diphenyldibutadiyne is < 1%.

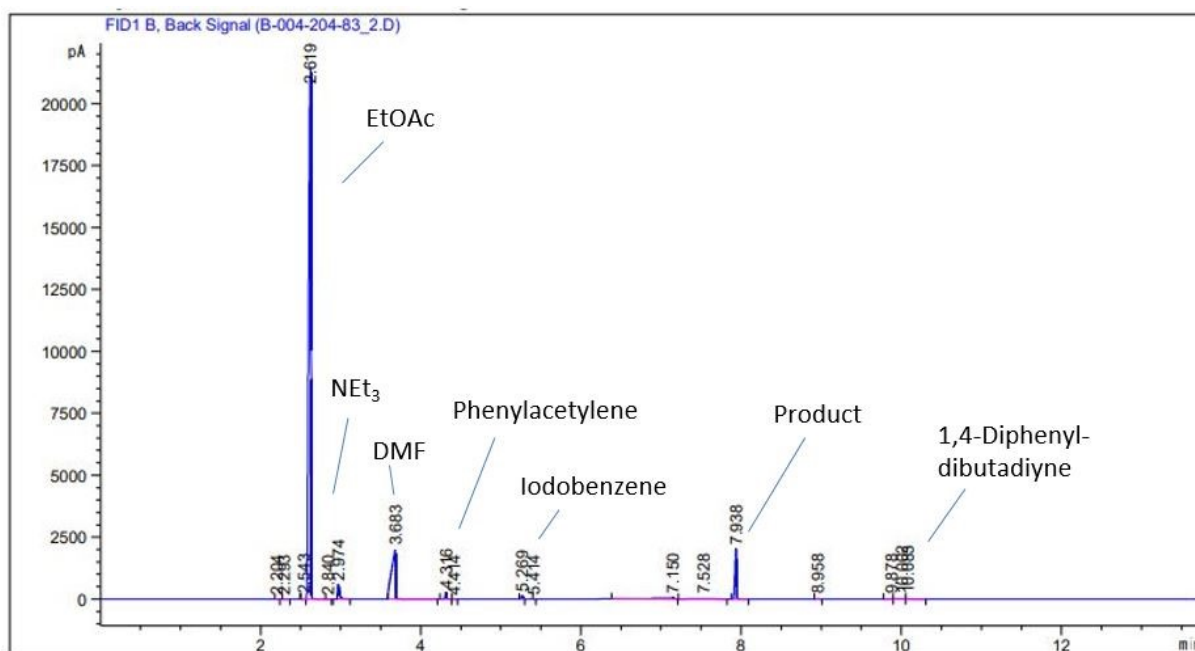


Figure S13 Exemplary GC run of the reaction mixture at almost full conversion.

NMR Spectroscopy

Nuclear magnetic resonance (NMR) spectra were recorded on a Varian Mercury 300 NMR spectrometer at 300 MHz for ¹H, ¹³C NMR, respectively. Solutions of reaction media (0.1 mL) diluted with CDCl₃-d₁ (0.4 mL) were measured immediately after preparation.

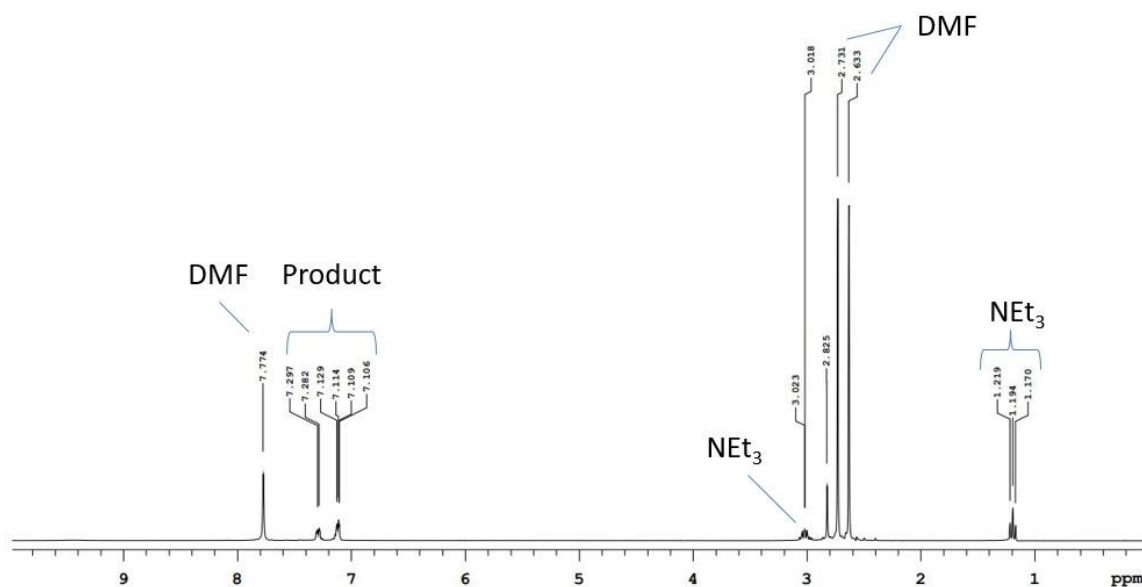


Figure S14 ¹H NMR spectra of the reaction mixture.

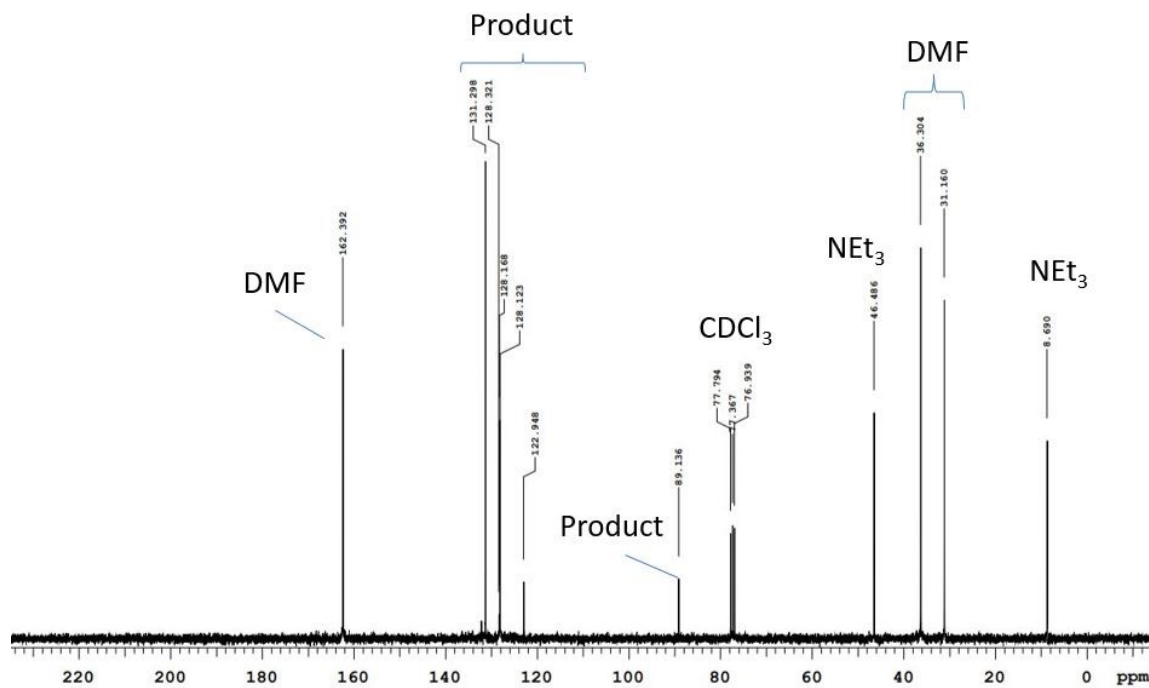


Figure S15 ^{13}C NMR spectra of the reaction mixture.

Abbreviations

c_0	initial concentration
c_i	concentration of compound i
C	heat capacity of reactor system and mass of reaction
C	Concentration profiles
D	experimental data matrix
d_{ij}	element of the experimental data matrix D
d	channel diameter
E	error matrix
e_{ij}	element of the error matrix E
E_A	activation energy
$EtOAc$	ethylacetate
GC	gas chromatography
$\Delta_R H$	reaction enthalpy
k	reaction rate coefficient
k_{ref}	reaction rate coefficient at reference temperature
LoF	lack of fit
MCR	multivariate curve resolution
R	ideal gas constant
R^2	variance explained
S^T	spectra of the involved components
t	time
t_{end}	overall experiment time
$t_{0.5}$	reaction halftime
T_{ref}	reference temperature

ΔT_{\max}	max. temperature rise
U	overall heat coefficient
V_d	delay volume
V_r	reactor volume
Q_0	initial flow rate
Q_{end}	final flow rate
α	residence time gradient
λ	thermal conductivity
τ_o	initial residence time
τ_{end}	final residence time

References

1. ACS GCI Pharmaceutical Roundtable, <https://www.acs.org/greenchemistry/research-innovation/tools-for-green-chemistry/solvent-tool.html>, **08.02.2023**.
2. V. Mazet, C. Carteret, D. Brie, J. Idier and B. Humbert, *Chemometrics and Intelligent Laboratory Systems*, 2005, **76**, 121.
3. B. Schrader, *Raman/infrared atlas of organic compounds*, VCH, Weinheim, 1989.
4. G. Taylor, *Proc. R. Soc. Lond. A*, 1953, **219**, 186.
5. R. Aris, *Proc. R. Soc. Lond. A*, 1956, **235**, 67.
6. P. Daskopoulos and A. M. Lenhoff, *AIChE J.*, 1988, **34**, 2052.
7. N. Kockmann, *Transport phenomena in micro process engineering: With 17 tables*, Springer, Berlin, Heidelberg, 2008.
8. T. Westermann and L. Mleczko, *Org. Process Res. Dev.*, 2016, **20**, 487.
9. K. G. JOBACK and R. C. REID, *Chemical Engineering Communications*, 1987, **57**, 233.
10. J. S. Moore and K. F. Jensen, *Angew. Chem.*, 2014, **126**, 480.
11. R. Tauler, A. Smilde and B. Kowalski, *J. Chemometrics*, 1995, **9**, 31.
12. M. Gazvoda, M. Virant, B. Pinter and J. Košmrlj, *Nature communications*, 2018, **9**, 4814.
13. R. Chinchilla and C. Nájera, *Chemical Society reviews*, 2011, **40**, 5084.
14. T. Rosner, J. Le Bars, A. Pfaltz and D. G. Blackmond, *Journal of the American Chemical Society*, 2001, **123**, 1848.
15. G. P. van F. Strijdonck, M. D. K. Boele, P. C. J. Kamer, J. G. de Vries and P. W. N. M. van Leeuwen, *Eur. J. Inorg. Chem.*, 1999, **1999**, 1073.